



Semiquantitative magnetic resonance imaging parameters for differentiating parotid pleomorphic adenoma from Warthin tumor

Shao-Nan He^{1,2#^}, Ren-Cai Lu^{3#^}, Jia-Long Zhou^{1,2}, Bo Wang^{1,2}, Guo-Li Bi^{1,2}, Kun-Hua Wu^{1,2^}

¹Magnetic Resonance Imaging Department, the First People's Hospital of Yunnan Province, Kunming, China; ²Magnetic Resonance Imaging Department, the Affiliated Hospital of Kunming University of Science and Technology, Kunming, China; ³PET-CT Center, the First People's Hospital of Yunnan Province, Kunming, China

Contributions: (I) Conception and design: SN He, RC Lu; (II) Administrative support: KH Wu; (III) Provision of study materials or patients: KH Wu; (IV) Collection and assembly of data: JL Zhou, B Wang; (V) Data analysis and interpretation: SN He, RC Lu; (VI) Manuscript writing: All authors; (VII) Final approval of manuscript: All authors.

#These authors contributed equally to this work.

Correspondence to: Kun-Hua Wu, MA. Magnetic Resonance Imaging Department, the First People's Hospital of Yunnan Province, Kunming 650032, China; Magnetic Resonance Imaging Department, the Affiliated Hospital of Kunming University of Science and Technology, 157 Jinbi Road, Kunming 650032, China. Email: wukunhua@hotmail.com.

Background: Accurately distinguishing between pleomorphic adenoma (PA) and Warthin tumor (WT) is beneficial for their respective management. Preoperative magnetic resonance imaging (MRI) can provide valuable information due to its excellent soft tissue contrast. This study explored the value of semiquantitative contrast-enhanced MRI parameters in the differential diagnosis of PA and WT.

Methods: Data from 106 patients, 62 with PA and 44 with WT (confirmed by histopathology) were retrospectively and consecutively analyzed. The tumor-to-spinal cord contrast ratios (TSc-CR) based on the mean, maximum, and minimum signal intensity (T_1 -mean TSc-CR, T_1 -max TSc-CR, and T_1 -min TSc-CR, respectively) in the early and delayed phases were calculated on contrast-enhanced T_1 -weighted images as semiquantitative parameters, and then compared between PA and WT. Receiver operating characteristic (ROC) curve analysis and areas under the curve (AUCs) were used to determine the performance of these parameters in the differential diagnosis of PA from WT.

Results: Except T_1 -min TSc-CR in the early phase, all semiquantitative MRI parameters differed significantly between PA and WT (all $P < 0.05$). T_1 -max TSc-CR showed higher sensitivity [70.45% [95% confidence interval (CI): 0.548–0.832]] and specificity [70.97% (95% CI: 0.581–0.818)] and had a higher AUC [0.707 (95% CI: 0.610–0.791)] in the early phase when using a cutoff value of 1.89. T_1 -max TSc-CR showed higher sensitivity [88.64% (95% CI: 0.754–0.962)], specificity [72.58% (95% CI: 0.598–0.831)], and AUC [0.854 (95% CI: 0.772–0.915)] in the delayed phase when using a cutoff value of 2.33. The sensitivity, specificity, and AUC were improved to 90.91% (95% CI: 0.783–0.975), 93.55% (95% CI: 0.843–0.982), and 0.960 (95% CI: 0.903–0.988), respectively, after combination of all semiquantitative parameters in the early and delayed phases. The two radiologists had excellent interobserver agreement on TSc-CRs [all interclass correlation coefficient (ICC) > 0.75].

Conclusions: Semiquantitative parameters using TSc-CR are valuable in distinguishing PA from WT, and a combination of these parameters can improve the differential diagnostic efficiency.

Keywords: Magnetic resonance imaging (MRI); adenoma; pleomorphic; Warthin tumor (WT)

[^] ORCID: Shao-Nan He, 0000-0002-4025-5409; Ren-Cai Lu, 0000-0002-2742-4108; Kun-Hua Wu, 0000-0003-3029-6140.

Submitted Jan 03, 2023. Accepted for publication Jul 19, 2023. Published online Jul 27, 2023.

doi: 10.21037/qims-22-1445

View this article at: <https://dx.doi.org/10.21037/qims-22-1445>

Introduction

The two most common benign salivary gland tumors are pleomorphic adenomas (PAs; benign mixed tumors) and Warthin tumors (WTs) (1). PAs account for most salivary gland tumors and are primarily found in the parotid gland (2). WTs are the second most common salivary gland tumor, and approximately 10–20% are found bilaterally in the parotid gland (3).

Appropriate management of WTs and PAs is important. PA has the potential for malignant transformation and a risk of recurrence, whereas WT is characterized by a slow growth rate (4,5). PA requires a partial parotidectomy, whereas WTs are treated only with local surgery or observation (4,6–8). Guidelines of the French Society of Otorhinolaryngology-Head and Neck Surgery (SFORL) recommended that complete *en bloc* tumor resection is necessary in case of preoperative suspicion of parotid PA (level of evidence, grade C) (9). Fine-needle aspiration cytology has been shown to be of considerable value in the diagnosis and management of lesions in the salivary gland, with high sensitivity ranging from 86% to 100% (10). However, fine-needle aspiration is invasive and challenges remain; for example, overlapping cytological features and multiple head and neck tumors may mislead cytologists (11). In addition, tumor recurrence by tumor seeding should be considered (12). Accurately distinguishing between WT and PA before surgery is beneficial for patients.

Preoperative magnetic resonance imaging (MRI) can provide important information because of its superior soft tissue contrast and thus reduce unnecessary biopsy of parotid tumors (13). However, conventional T₁-weighted imaging (T₁WI) and T₂-weighted imaging (T₂WI) is not sufficient to distinguish between WT and PA for its variability of histological components of PA (14,15). Magnetic resonance (MR) techniques such as dynamic contrast-enhanced MRI and diffusion-weighted (DW) MRI have been used to differentiate parotid neoplasms (16). Although researchers have developed a range of methods based on MRI to distinguish these two diseases (17,18), there is scarce literature reporting the value of early and delayed contrast-enhanced MRI in differentiating WT and PA. In the present study, we used the relatively stable signal intensity of the spinal cord as a reference and calculated

the tumor-to-spinal cord contrast ratio (TSc-CR) in early and delayed phases to establish useful semiquantitative parameters and then explored the use of these parameters in differentiating PAs from WTs. We present this article in accordance with the STARD reporting checklist (available at <https://qims.amegroups.com/article/view/10.21037/qims-22-1445/rc>).

Methods

Patients

This study retrospectively and consecutively analyzed the clinical data and MRI examination results of 106 patients with PA and WT who presented to First People's Hospital of Yunnan Province between January 2015 and October 2020. All patients underwent MRI examinations, with their condition pathologically confirmed following surgical resection.

To be eligible for inclusion criteria in this study, patients had to meet the following criteria: (I) parotid lesions had not been treated with puncture biopsy, radiotherapy, or chemotherapy prior to MRI examinations; (II) MRI images met diagnostic quality requirements and were complete in three directions (transverse, coronal, and sagittal) after contrast enhancement; (III) definitive pathological and histological findings were available. The exclusion criteria are presented in *Figure 1*.

The present study was conducted in accordance with the Declaration of Helsinki (as revised in 2013). The study was approved by the Ethics Committee of the First People's Hospital of Yunnan Province (No. KHLL2022-KY176). The requirement for informed consent from all patients was waived due to the retrospective nature of this study.

MRI imaging techniques

MRI examinations were performed within 1 month before surgery in all patients. Patients were examined using a Signa HDxt 3.0T (GE Healthcare, Chicago, IL, USA), MAGNETOM Prisma 3.0T (Siemens Healthcare, Erlangen, Germany), Siemens Aera 1.5T (Siemens Healthcare), or 1.5T Ingenia MRI scanner (Philips Medical Systems, Best, Netherlands), with an integrated

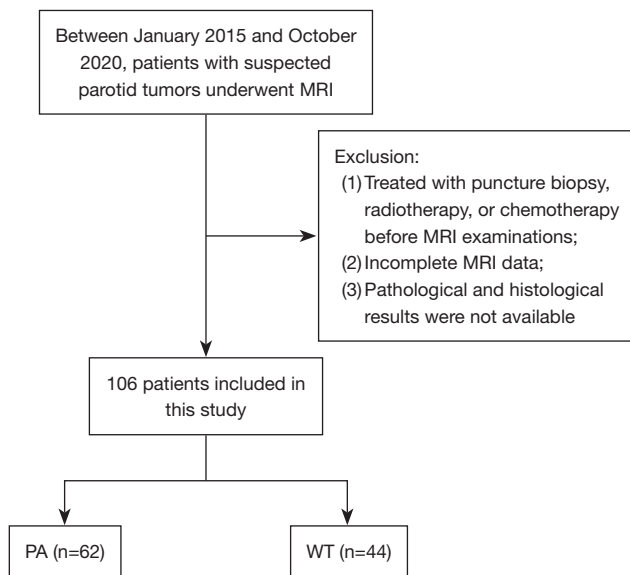


Figure 1 Flowchart of case selection and distribution in this study. MR, magnetic resonance; MRI, magnetic resonance imaging; PA, pleomorphic adenoma; WT, Warthin tumor.

head and neck coil. All patients underwent preoperative conventional MRI scanning; a post enhancement T_1 WI three-dimensional (3D) scan (transverse, coronal, and sagittal) was performed after administration of 0.1 mmol/kg gadolinium-diethylenetriamine penta-acetic acid (Gd-DTPA) at a rate of 2.0 mL/s followed by a 20 mL saline flush into the antecubital vein. Acquisition series included coronal short tau inversion recovery (STIR) T_2 WI [repetition time (TR), 3,500 ms; time to echo (TE), 80 ms] and fast spin-echo (FSE) T_1 WI (TR, 500 ms; TE, 20 ms), and transverse STIR T_2 WI (TR, 3,500 ms; TE, 80 ms) and gradient echo sequences (GRE) T_1 WI (TR, 6 ms; TE, 2 ms); enhanced images were scanned with GRE T_1 WI. MRI images were obtained at a section thickness of 4 mm, an effective layer interval of 2 mm, a 512×512 matrix, and a field of view of 280×280 mm. The early phase was defined as the first transverse sequence acquired after injection of Gd-DTPA, and the delayed phase was defined as the third sagittal sequence acquired after injection of Gd-DTPA (at approximately 3 min).

Image analysis

MRI data were transferred to a syngo.via workstation (Client 4.2; Siemens Healthineers, Erlangen, Germany). Images were reviewed by two experienced radiologists (BW and

JLZ, with 26 and 5 years of MRI diagnostic experience in the head and neck, respectively). The mean, maximum, and minimum signal intensity of the tumor and spinal cord at the same level were measured on contrast-enhanced T_1 WI. Regions of interest (ROIs) were drawn freehand as large as possible, including the solidly enhancing component of the tumor, in PA and WT lesions, avoiding necrotic cystic areas and larger vessels. The ROI size was adjusted to ensure that it could cover the tumor and the selected ROIs were kept as consistent as possible. The central canal was avoided when measuring the signal intensity of the spinal cord. Based on the mean, maximum, and minimum signal intensity, TSc-CRs were calculated (T_1 -mean TSc-CR, T_1 -max TSc-CR, and T_1 -min TSc-CR, respectively) in the early and delayed phases. Interobserver consistency analysis of TSc-CRs measured by two radiologists was performed. The mean value of TSc-CRs was used for further analysis.

Statistical analysis

All statistical analyses were performed using MedCalc 18.2.1 (MedCalc Software Ltd., Ostend, Belgium; <https://www.medcalc.org/>). The normality of data distribution was checked using the Kolmogorov-Smirnov test. Data that were normally distributed were presented as the mean \pm standard deviation (SD) and compared using Student's *t*-test. Data that were not normally distributed were presented as the median with interquartile range and were compared using the Mann-Whitney test. Receiver operating characteristic (ROC) curve analysis and areas under the curve (AUCs) were used to determine the performance of the parameters (TSc-CRs) in differentiating PAs from WTs. DeLong test was used to compare performance differences between ROCs. The sensitivity, specificity, and accuracy for differentiating PAs and WTs were calculated. A two-tailed $P < 0.05$ was considered statistically significant. Inter-observer agreement of TSc-CRs measured by two radiologists were evaluated by the interclass correlation coefficient (ICC) analysis, ICC value > 0.75 was considered a mark of excellent reliability.

Results

Clinical data

Of these 106 patients, 62 (21 males, 41 females) had PA and 44 (43 males, 1 female) had WT. The mean age of patients with PA was 39.7 years (range, 16–75 years), and the disease

Table 1 Clinical data for patients in the PA and WT groups

Characteristics	Histopathologic diagnosis		t/ χ^2	P value
	PA (n=62)	WT (n=44)		
Gender			43.866	<0.001 [†]
Male	21 (33.87)	43 (97.73)		
Female	41 (66.13)	1 (2.27)		
Age (years)	39.69±14.78	55.70±9.21	6.856	<0.001 [†]
Smoking history	7 (11.29)	40 (90.91)	66.105	<0.001 [†]
Location			4.391	0.111 [†]
Deep lobe	2 (32.25)	0 (0.00)		
Superficial lobe	40 (64.52)	22 (50.00)		
Across deep and superficial lobes	20 (32.26)	22 (50.00)		
Shape			13.989	<0.001 [†]
Regular	53 (85.48)	23 (52.27)		
Irregular	9 (14.52)	21 (47.73)		
Longest diameter			2.763	0.096 [†]
<30 mm	60 (96.77)	39 (88.64)		
≥30 mm	2 (3.23)	5 (11.36)		
High signal on T ₂ WI	32 (51.61)	40 (90.91)	18.241	<0.001 [†]
Delayed enhancement capsular	61 (98.39)	2 (4.55)	94.001	<0.001 [†]
Local T ₂ WI low signal	5 (8.06)	6 (13.64)	–	0.520 [§]
Number of lesions			4.211	0.040 [†]
Single lesion	42 (67.74)	20 (45.45)		
Multiple lesions	20 (32.26)	22 (50.00)		
Accompanied by pain	5 (8.06)	1 (2.27)		0.397 [§]

Unless indicated otherwise, data are given as the mean ± SD or n (%). [†], χ^2 test; [‡], Student's *t*-test; [§], Fisher's exact test. PA, pleomorphic adenoma; WT, Warthin tumor; T₂WI, T₂-weighted imaging; SD, standard deviation.

durations ranged from 1 week to 20 years. The mean age of patients with WT was 59.7 years (range, 36–76 years), and the disease durations ranged from 10 days to 20 years. All patients presented with painless progressive enlargement of the mass clinically, except for 3 patients with pain; 40 patients had a history of smoking. As indicated in *Table 1*, compared with PA patients, WT patients were older, more likely to be male, and more likely to have a history of smoking (all *P*<0.05). PAs were more likely to have a regular shape, show delayed capsular enhancement (a circular, homogeneous, and highly enhanced linear enhancement around the lesion in the delayed phase), and consist of a single lesion (all *P*<0.05), whereas high signal on T₂WI

was often seen in WTs (*P*<0.05). There were no significant differences in lesion location or longest diameter, the number of patients with local T₂WI-low signals patients, or the localized pain symptoms between the two groups (all *P*>0.05; *Table 1*).

Comparison of semiquantitative MRI parameters between the PA and WT groups

The two radiologists demonstrated excellent interobserver agreement on T₁-max TSc-CR [early phase: ICC =0.994, 95% confidence interval (CI): 0.991–0.996; delayed phase: ICC =0.996, 95% CI: 0.994–0.997], T₁-mean TSc-CR

Table 2 Comparison of semiquantitative MRI parameters between the PA and WT groups

Semiquantitative MRI parameters	PA (n=62)	WT (n=44)	Z	P value
Early phase				
T ₁ -mean TSc-CR	1.722 (1.467–2.191)	1.490 (1.325–1.839)	–2.411	0.016
T ₁ -max TSc-CR	2.160 (1.767–2.864)	1.706 (1.469–2.018)	–3.616	<0.001
T ₁ -min TSc-CR	1.281 (1.097–1.642)	1.292 (1.179–1.624)	–0.840	0.401
Delayed phase				
T ₁ -mean TSc-CR	2.320 (1.872–3.066)	1.473 (1.282–1.796)	–6.072	<0.001
T ₁ -max TSc-CR	2.709 (2.093–3.478)	1.626 (1.441–1.962)	–6.181	<0.001
T ₁ -min TSc-CR	1.758 (1.523–2.216)	1.269 (1.114–1.590)	–4.988	<0.001

Unless indicated otherwise, data are given as the median (interquartile range). Comparisons were made using the Mann-Whitney test. The semiquantitative parameters were based MRI and included the TSc-CR based on the mean, maximum, and minimum signal intensity (T₁-mean TSc-CR, T₁-max TSc-CR, and T₁-min TSc-CR, respectively). MRI, magnetic resonance imaging; PA, pleomorphic adenoma; WT, Warthin tumor; TSc-CR, tumor-to-spinal cord contrast ratio.

(early phase: ICC =0.995, 95% CI: 0.994–0.997; delayed phase: ICC =0.998, 95% CI: 0.997–0.998), T₁-min TSc-CR (early phase: ICC =0.986, 95% CI: 0.979–0.990; delayed phase: ICC =0.990, 95% CI: 0.986–0.993). There were significant (P<0.05) differences in all semiquantitative MRI parameters between the PA and WT groups, except for T₁-min TSc-CR in the early phase (P=0.401; Table 2, Figures 2A–2E, 3A–3E).

ROC curve analysis of MRI parameters in the early phase

When early phase parameters were used alone to identify the two diseases, significant differences were found for T₁-mean TSc-CR and T₁-max TSc-CR (P=0.0126 and P=0.0001, respectively). The sensitivity (81.82%) and specificity (88.71%) increased after combination of the three parameters, with a Youden index of 0.7053. The AUC (0.912) was improved, and there was a significant difference between the PA and WT groups using the combination of T₁-mean TSc-CR, T₁-max TSc-CR, and T₁-min TSc-CR in the early phase (P<0.001; Table 3, Figure 4).

ROC curve analysis of MRI parameters in the delayed phase

Individually, all MRI parameters in the delayed phase differed significantly (P<0.05) between the two diseases. After the combination of the three parameters, the sensitivity (81.82%) decreased compared with T₁-mean TSc-CR and T₁-max TSc-CR, the specificity (83.87%)

increased, and the Youden index was 0.6569. The AUC improved [0.892 (95% CI: 0.817–0.944)] and there was a statistically difference with T₁-mean TSc-CR (P=0.0059; Table 4, Figure 5).

Diagnostic efficiency of the combination of all MRI parameters

As shown in Figure 6, when all early and delayed phase semiquantitative parameters were combined, the diagnostic efficacy was better than the combination of early or delayed MR parameters alone [sensitivity 90.91% (95% CI: 0.783–0.975), specificity 93.55% (95% CI: 0.843–0.982), Youden index 0.8446]. In ROC curve analysis, the AUC was 0.960 (Z=25.504, P<0.0001, 95% CI: 0.903–0.988; Figure 5), with a significant difference compared with the combination of only early phase MRI parameters (P=0.0495) or delayed phase MRI parameters (P=0.0068, DeLong test).

Discussion

Age, gender, and smoking history in WT and PA patients showed statistical differences, but were not sufficient to distinguish the two diseases (19). In the present study, the age, number of male patients, and number of patients who smoked were higher in the WT than PA group (Table 1), findings that are similar to those reported by Luers *et al.* (5) On MRI, most PA are solitary, round, and well circumscribed with a smooth but sometimes lobulated surface. They have homogeneous bright and high-intensity

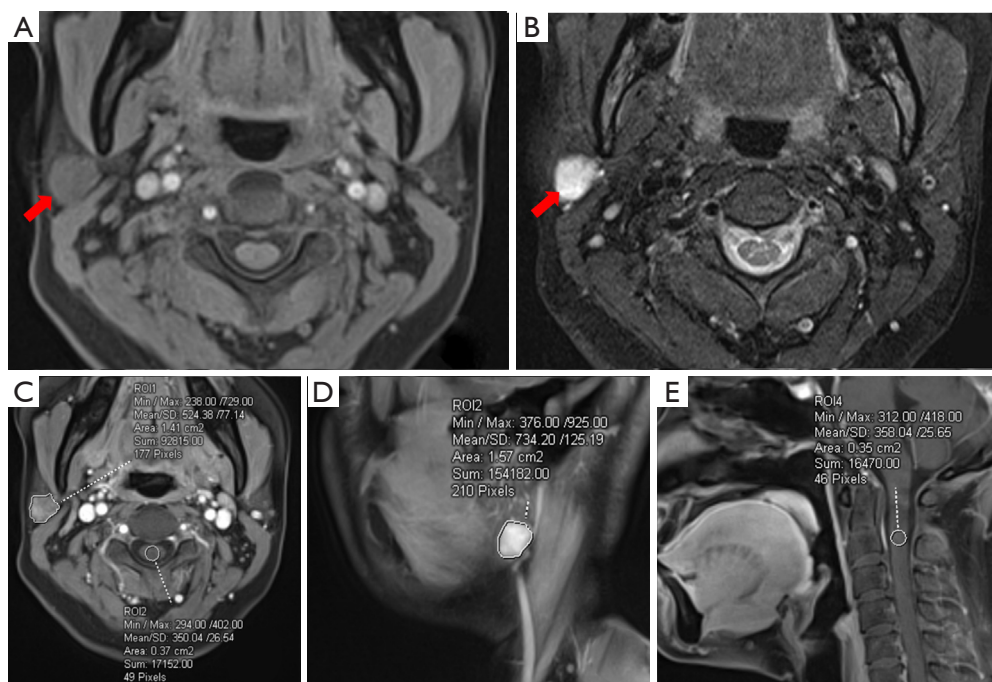


Figure 2 Typical images of the ROIs in a patient with PA. This patient was a 42-year-old woman in whom parotid nodules had gradually increased in size over a period of 3 years. (A,B) The imaging findings were isointensity on non-contrast T₁-weighted images (A; arrow) and hyperintensity on T₂-weighted images (B; arrow). (C-E) ROIs were placed in the parotid lesion and spinal cord on early (C) and delayed (D,E) phase MR images, and semiquantitative parameters were calculated, namely the TSc-CR based on the mean, maximum, and minimum signal intensity (T₁-mean TSc-CR, T₁-max TSc-CR, and T₁-min TSc-CR, respectively). (C) In the early phase, the T₁-mean TSc-CR was 1.50, T₁-max TSc-CR was 2.08, and T₁-min TSc-CR was 0.70. (D,E) In the delayed phase, T₁-mean TSc-CR was 2.06, T₁-max TSc-CR was 2.61, and T₁-min TSc-CR was 1.06. ROI, region of interest; SD, standard deviation; PA, pleomorphic adenoma; MR, magnetic resonance; TSc-CR, tumor-to-spinal cord contrast ratio.

signals, with localized bright signals representing myxoid tissue on T₂WI (20). MRI features, such as low signal intensity on T₂WI represent highly cellular tumors, with multiple and bilateral lesions, well-circumscribed or partly solid lesions, and a location in the tail of parotid gland, being considered as the characteristic features (21). However, PA and WT cannot be distinguished on the basis of conventional T₂WI signals alone (15) (Figures 2A-2E, 3A-3E). The variable amounts of extracellular stroma, epithelial cells, and myoepithelial cells, constitutes the histological manifestation of PA, but overlaps with other benign and malignant parotid neoplasms in MRI findings (14).

Noninvasive medical imaging techniques are essential for distinguishing between parotid tumors. MRI is widely used in the differentiation of parotid gland tumors because of its high soft tissue resolution. Contrast-enhanced MRI enables additional evaluation of the perineural spread of aggressive lesions along the facial nerve (22). Multiparametric MRI and

dynamic contrast-enhanced MRI can be used to distinguish between malignant and benign parotid tumors (23,24).

Preoperative differentiation between PA and WT is necessary because of differences in the malignant transformation potential and treatment of these two diseases. Liu *et al.* (25) reported that FSE diffusion-weighted imaging (DWI) with periodically rotated overlapping parallel lines with enhanced reconstruction was helpful in distinguishing PA from WT with less distortion of the tumors, but the signal-to-noise ratio and AUC were lower than those of single-shot echo-planar DWI. DWI and apparent diffusion coefficient (ADC) are potentially useful to evaluate salivary tumors, however, the mean ADCs between salivary gland tumors still have some overlap (26-28). In another study, Wang *et al.* (18) developed a WT scoring system by combining the mean and SD of the ADC of tumors, patient age, and patient sex to differentiate WTs from other parotid PAs and carcinomas. Their scoring

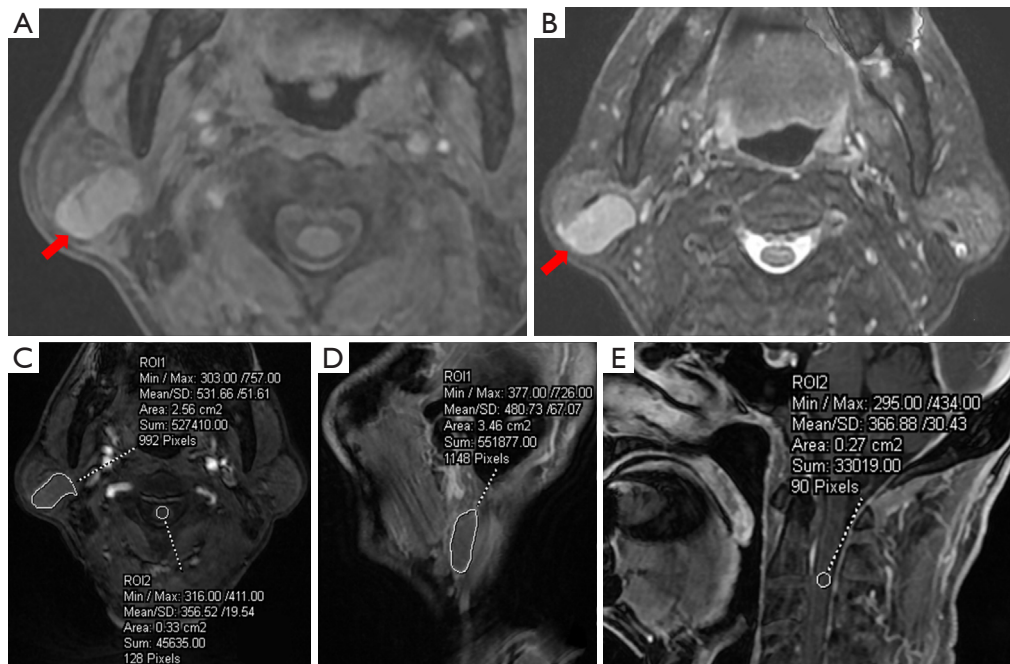


Figure 3 Typical images of the ROIs in patient with WT. This patient was a 65-year-old man who had had painless parotid nodules for 1 year. (A,B) The imaging findings showed slight hyperintensity on non-contrast T₁-weighted images (A; arrow) and hyperintensity on T₂-weighted images (B; arrow). (C-E) ROIs were placed in the parotid lesion and spinal cord on early (C) and delayed (D,E) phase MR images and semiquantitative parameters were calculated, namely the TSc-CR based on the mean, maximum, and minimum signal intensity (T₁-mean TSc-CR, T₁-max TSc-CR, and T₁-min TSc-CR, respectively). (C) In the early phase, the T₁-mean TSc-CR was 1.49, T₁-max TSc-CR was 2.12, and T₁-min TSc-CR was 0.85. (D,E) In the delayed phase, the T₁-mean TSc-CR was 1.31, T₁-max TSc-CR was 1.98, and T₁-min TSc-CR was 1.03. ROI, region of interest; SD, standard deviation; WT, Warthin tumor; MR, magnetic resonance; TSc-CR, tumor-to-spinal cord contrast ratio.

Table 3 Diagnostic efficiency of the TSc-CR in the early phase to differentiate PAs and WTs

Semiquantitative MRI parameters	T ₁ -mean TSc-CR	T ₁ -max TSc-CR	T ₁ -min TSc-CR	Combination of all 3 parameters
Sensitivity (%) (95% CI)	70.45 (0.548–0.832)	70.45 (0.548–0.832)	77.27 (0.622–0.885)	81.82 (0.673–0.918)
Specificity (%) (95% CI)	66.13 (0.530–0.777)	70.97 (0.581–0.818)	40.32 (0.281–0.536)	88.71 (0.781–0.953)
Youden index	0.3658	0.4142	0.1760	0.7053
Cutoff value	1.62	1.89	1.16	–
ROC curve analysis				
AUC (95% CI)	0.638 (0.539–0.729)	0.707 (0.610–0.791)	0.547 (0.448–0.644)	0.912 (0.841–0.958)
SE [†]	0.0553	0.0516	0.0563	0.0274
Z	2.494	4.004	0.843	15.014
P value	0.0126	0.0001	0.3994	<0.0001

[†], DeLong test. The AUC for the combination of the TSc-CR based on the mean, and maximum, minimum signal intensity (T₁-mean TSc-CR, T₁-max TSc-CR, and T₁-min TSc-CR, respectively) compared with the AUC for each parameter alone differed significantly (P<0.0001). TSc-CR, tumor-to-spinal cord contrast ratio; PA, pleomorphic adenoma; WT, Warthin tumor; MRI, magnetic resonance imaging; ROC, receiver operating characteristic; AUC, area under the curve; SE, standard error; CI, confidence interval.

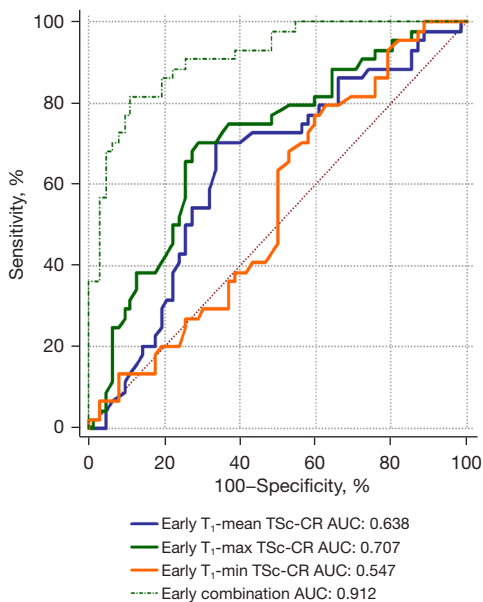


Figure 4 ROC analysis of MRI parameters in the early phase. The AUC improved (0.912) after combination of the early phase TSc-CRs based on the mean, maximum, and minimum signal intensity (T₁-mean TSc-CR, T₁-max TSc-CR, and T₁-min TSc-CR, respectively). TSc-CR, tumor-to-spinal cord contrast ratio; AUC, area under the curve; ROC, receiver operating characteristic; MRI, magnetic resonance imaging.

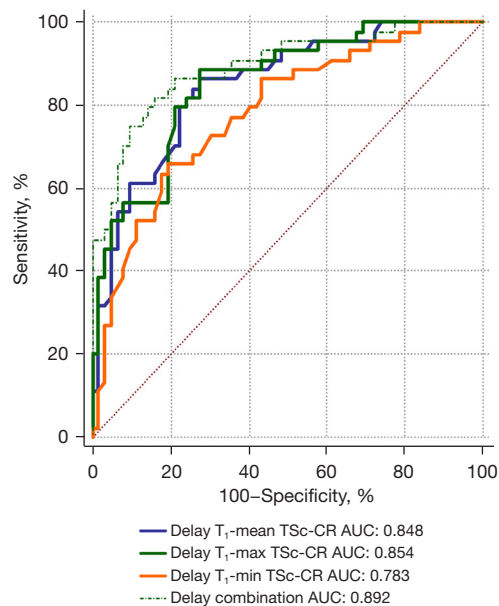


Figure 5 ROC curve analysis of MRI parameters in the delayed phase. The AUC improved (0.892) after combination of the delayed phase TSc-CRs based on the mean, maximum, and minimum signal intensity (T₁-mean TSc-CR, T₁-max TSc-CR, and T₁-min TSc-CR, respectively). TSc-CR, tumor-to-spinal cord contrast ratio; AUC, area under the curve; ROC, receiver operating characteristic; MRI, magnetic resonance imaging.

Table 4 Diagnostic efficiency of the TSc-CR in the delayed phase in differentiating PAs from WTs

Semiquantitative MRI parameters	T ₁ -mean TSc-CR	T ₁ -max TSc-CR	T ₁ -min TSc-CR	Combination of all 3 parameters
Sensitivity (%) (95% CI)	86.36 (0.726–0.948)	88.64 (0.754–0.962)	65.91 (0.501–0.795)	81.82 (0.673–0.918)
Specificity (%) (95% CI)	72.58 (0.598–0.831)	72.58 (0.598–0.831)	80.65 (0.686–0.896)	83.87 (0.723–0.920)
Youden index	0.5894	0.6122	0.4655	0.6569
Cutoff value	1.95	2.33	1.44	–
ROC curve analysis				
AUC (95% CI)	0.848 (0.765–0.910)	0.854 (0.772–0.915)	0.783 (0.693–0.857)	0.892 (0.817–0.944)
SE [†]	0.0378	0.0365	0.0452	0.0325
Z	9.205	9.680	6.269	12.081
P value	<0.0001	<0.0001	<0.0001	<0.0001

[†], DeLong test. The AUC for the combination of the TSc-CR based on the mean, maximum, and minimum signal intensity (T₁-mean TSc-CR, T₁-max TSc-CR, and T₁-min TSc-CR, respectively) compared with the AUC for T₁-mean TSc-CR differed significantly (P=0.0059). TSc-CR, tumor-to-spinal cord contrast ratio; PA, pleomorphic adenoma; WT, Warthin tumor; MRI, magnetic resonance imaging; ROC, receiver operating characteristic; AUC, area under the curve; SE, standard error; CI, confidence interval.

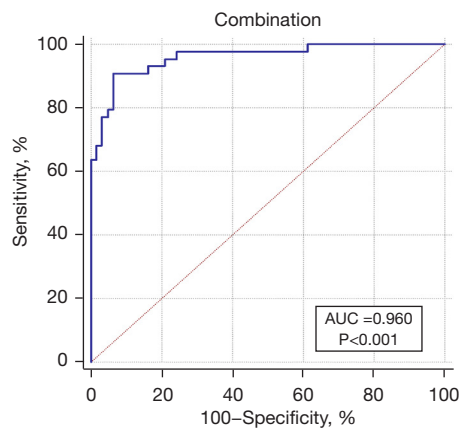


Figure 6 The ROC curve had an AUC of 0.960 after combination of all early and delayed phase semiquantitative MRI parameters. AUC, area under the curve; ROC, receiver operating characteristic; MRI, magnetic resonance imaging.

system was shown to have a high differential diagnostic performance, with high sensitivity (85.7%), specificity (100.0%), and accuracy (93.4%) (18). Nevertheless, the low sample size (78 patients in total, including 42 WTs, 30 PAs, and 20 carcinomas) may limit the generalizability of their conclusions (18). MRI-based radiomics and texture analysis has become an area of intense research interest and shows considerable application prospects (29–31). Gabelloni *et al.* (29) used a support vector machine classifier to differentiate between malignant and benign parotid neoplasms on T_2 WI, with high sensitivity (0.8695), specificity (0.9062), and accuracy (0.8909) in distinguishing PA from WT. However, the application of radiomics or deep learning is complicated and large datasets are required; image segmentation was based on visual inspection and manual delineation was time-consuming and laborious (32,33). The widespread application of radiomics in clinical practice needs to be further optimized.

There is a paucity of literature on semiquantitative parameters to differentiate PA from WT. In this study, we set the spinal cord signal at the same level for internal reference because the solidly enhanced components of the spinal cord were easy to acquire, there was smaller human measurement error, and signal interference from fat tissue in the parotid gland itself could be avoided (34). Relatively stable semiquantitative parameters can be obtained even if different MRI scanners are used, and misinterpretation caused by personal subjective experience may also be avoided to the greatest extent. In the present study, all

semiquantitative parameters, except T_1 -min TSc-CR in the early phase, were higher in PAs than in WTs (all $P < 0.05$), with the difference being more pronounced in the delayed phase (Table 2). This is possibly caused by the rapid wash-in and wash-out pattern of WTs, whereas a slow and progressive wash-in pattern is seen in PAs (21,22,35). The enhancement pattern ultimately resulted in a higher TSc-CR in PAs than in WTs. In the delayed phase, the difference between the slow progressive wash-in of PAs and the rapid wash-out of WTs became more pronounced, increasing the difference in TSc-CR between the two tumor types.

Wei *et al.* (17) also used TSc-CR to differentiate PA, WT, and malignant parotid tumors, and showed that the TSc-CR of WT was higher than that of PA, but they only measured semiquantitative MRI parameters on nonenhanced T_1 WI. Matsusue *et al.* (34) investigated the differences in ADC and TSc-CR among PA, WT, and parotid malignant tumors on T_1 WI, T_2 WI, and Gd-enhanced T_1 WI, also showing that the TSc-CR of PA on Gd-enhanced MRI was higher than that of WT, similar to the findings in the present study. However, Matsusue *et al.* (34) only enrolled 15 patients with PA and 17 patients with WT in their study, and the parameters of contrast-enhanced MRI were not abundant, meaning that their conclusion requires further validation through other studies. To obtain better parameters to distinguish between PA and WT, we focused on measuring the signal intensity ratio of all semiquantitative parameters to that of the spinal cord on enhanced MRI. In most cases, the TSc-CRs in PA and WT differed significantly. Since these parameters can be easily and rapidly measured in clinical practice, they could provide valuable clinical information.

This study further explored the diagnostic performance of semiquantitative MRI parameters in differentiating PA from WT. The results showed that the TSc-CR measured from the T_1 -max value in the early or delayed phase had a high differential diagnostic efficiency (AUC 0.707 and 0.854, respectively). When all TSc-CRs in the early phase were combined, the diagnostic efficacy was improved, with a sensitivity, specificity, and AUC of 81.82%, 88.71%, and 0.912, respectively. The diagnostic efficacy of the combination of all delayed phase TSc-CRs was also improved, with a sensitivity, specificity, and AUC of 81.82%, 83.87%, and 0.892, respectively (Tables 3,4, Figures 4,5). When all early and delayed TSc-CRs were combined, the sensitivity, specificity, and AUC of the ROC curve were improved to 90.91%, 93.55%, and 0.960, respectively (Figure 5). These results indicate that semiquantitative MRI

parameters can be used to characterize PA and WT.

This study had several limitations. First, the sample size was small, only patients with PA and WT were included, and malignant parotid neoplasms were not analyzed due to its low incidence and wide variety; the study results may have been different if parotid malignancies had been included. Second, we used the signal intensity of the spinal cord as a reference, which may not yield reliable results in patients with spinal cord disease or in those with contraindications to the use of Gd-DTPA. Third, a standard neck contrast-enhanced MRI protocol was used instead of dynamic contrast-enhanced MRI or isotropic high-resolution post-contrast sequences, and the TSc-CRs of nonenhanced MRI, T₂WI, and DWI were not measured or analyzed. However, based on the above limitations and advantages, this study could be considered a preliminary pilot study because it introduces a set of semiquantitative parameters obtained using standard Gd-enhanced MRI sequences. In addition, the determination of these semiquantitative parameters is feasible and easy to implement in clinical practice, making them conducive to clinical application.

Conclusions

TSc-CRs on Gd-based contrast-enhanced MRI in the early and delayed phases are valuable for the differential diagnosis of PA and WT. The combined application of all semiquantitative parameters improves differential diagnostic performance.

Acknowledgments

Funding: This work was supported by the Basic Research on Application of Joint Special Funding of Science and Technology Department of Yunnan Province-Kunming Medical University (No. 202101AY070001-243) and the Kunming University of Science and Technology & the First People's Hospital of Yunnan Province Joint Special Project on Medical Research (No. KUST-KH2022026Y).

Footnote

Reporting Checklist: The authors have completed the STARD reporting checklist. Available at <https://qims.amegroups.com/article/view/10.21037/qims-22-1445/rc>

Conflicts of Interest: All authors have completed the ICMJE uniform disclosure form (available at <https://qims.amegroups.com/article/view/10.21037/qims-22-1445/coif>).

The authors have no conflicts of interest to declare.

Ethical Statement: The authors are accountable for all aspects of the work in ensuring that questions related to the accuracy or integrity of any part of the work are appropriately investigated and resolved. This present study was conducted in accordance with the Declaration of Helsinki (as revised in 2013). The study was approved by the Ethics Committee of the First People's Hospital of Yunnan Province (No. KHLL2022-KY176), and individual consent for this retrospective analysis was waived.

Open Access Statement: This is an Open Access article distributed in accordance with the Creative Commons Attribution-NonCommercial-NoDerivs 4.0 International License (CC BY-NC-ND 4.0), which permits the non-commercial replication and distribution of the article with the strict proviso that no changes or edits are made and the original work is properly cited (including links to both the formal publication through the relevant DOI and the license). See: <https://creativecommons.org/licenses/by-nc-nd/4.0/>.

References

1. Colella G, Cannavale R, Flamminio F, Foschini MP. Fine-needle aspiration cytology of salivary gland lesions: a systematic review. *J Oral Maxillofac Surg* 2010;68:2146-53.
2. Eveson JW, Cawson RA. Salivary gland tumours. A review of 2410 cases with particular reference to histological types, site, age and sex distribution. *J Pathol* 1985;146:51-8.
3. Klijanienko J, Vielh P. Fine-needle sampling of salivary gland lesions. II. Cytology and histology correlation of 71 cases of Warthin's tumor (adenolymphoma). *Diagn Cytopathol* 1997;16:221-5.
4. Song LL, Chen SJ, Chen W, Shi Z, Wang XD, Song LN, Chen DS. Radiomic model for differentiating parotid pleomorphic adenoma from parotid adenolymphoma based on MRI images. *BMC Med Imaging* 2021;21:54.
5. Luers JC, Guntinas-Lichius O, Klusmann JP, Küsgen C, Beutner D, Grosheva M. The incidence of Warthin tumours and pleomorphic adenomas in the parotid gland over a 25-year period. *Clin Otolaryngol* 2016;41:793-7.
6. Comoglu S, Ozturk E, Celik M, Avci H, Sonmez S, Basaran B, Kiyak E. Comprehensive analysis of parotid mass: A retrospective study of 369 cases. *Auris Nasus Larynx* 2018;45:320-7.
7. Mikaszewski B, Markiet K, Smugała A, Stodulski

- D, Szurowska E, Stankiewicz C. An algorithm for preoperative differential diagnostics of parotid tumours on the basis of their dynamic and diffusion-weighted magnetic resonance images: a retrospective analysis of 158 cases. *Folia Morphol (Warsz)* 2018;77:29-35.
8. Aro K, Korpi J, Tarkkanen J, Mäkitie A, Atula T. Preoperative evaluation and treatment consideration of parotid gland tumors. *Laryngoscope Investig Otolaryngol* 2020;5:694-702.
 9. Vergez S, Fakhry N, Cartier C, Kennel T, Courtade-Saidi M, Uro-Coste E, Varoquaux A, Righini CA, Malard O, Mogultay P, Thariat J, Tronche S, Garrel R, Chevalier D. Guidelines of the French Society of Otorhinolaryngology-Head and Neck Surgery (SFORL), part I: Primary treatment of pleomorphic adenoma. *Eur Ann Otorhinolaryngol Head Neck Dis* 2021;138:269-74.
 10. Rossi ED, Faquin WC. The Milan System for Reporting Salivary Gland Cytopathology (MSRSGC): An international effort toward improved patient care-when the roots might be inspired by Leonardo da Vinci. *Cancer Cytopathol* 2018;126:756-66.
 11. Tyagi R, Dey P. Diagnostic problems of salivary gland tumors. *Diagn Cytopathol* 2015;43:495-509.
 12. Eisele DW, Bradley PJ. Salivary Gland Neoplasms: Future Perspectives. *Adv Otorhinolaryngol* 2016;78:198-9.
 13. Alibek S, Zenk J, Bozzato A, Lell M, Grunewald M, Anders K, Rabe C, Iro H, Bautz W, Greess H. The value of dynamic MRI studies in parotid tumors. *Acad Radiol* 2007;14:701-10.
 14. Zoghi S, Hendizadeh L, Hung T, Farahvar S, Abemayor E, Sepahdari AR. MRI criteria for the diagnosis of pleomorphic adenoma: a validation study. *Am J Otolaryngol* 2014;35:713-8.
 15. Sakamoto M, Sasano T, Higano S, Takahashi S, Iikubo M, Kakehata S. Usefulness of heavily T(2) weighted magnetic resonance images for the differential diagnosis of parotid tumours. *Dentomaxillofac Radiol* 2003;32:295-9.
 16. Kato H, Kanematsu M, Watanabe H, Kajita K, Mizuta K, Aoki M, Okuaki T. Perfusion imaging of parotid gland tumours: usefulness of arterial spin labeling for differentiating Warthin's tumours. *Eur Radiol* 2015;25:3247-54.
 17. Wei PY, Shao C, Huan T, Wang HB, Ding ZX, Han ZJ. Diagnostic value of maximum signal intensity on T1-weighted MRI images for differentiating parotid gland tumours along with pathological correlation. *Clin Radiol* 2021;76:472.e19-25.
 18. Wang CW, Chu YH, Chiu DY, Shin N, Hsu HH, Lee JC, Juan CJ. JOURNAL CLUB: The Warthin Tumor Score: A Simple and Reliable Method to Distinguish Warthin Tumors from Pleomorphic Adenomas and Carcinomas. *AJR Am J Roentgenol* 2018;210:1330-7.
 19. Patel DK, Morton RP. Demographics of benign parotid tumours: Warthin's tumour versus other benign salivary tumours. *Acta Otolaryngol* 2016;136:83-6.
 20. Tsushima Y, Matsumoto M, Endo K, Aihara T, Nakajima T. Characteristic bright signal of parotid pleomorphic adenomas on T2-weighted MR images with pathological correlation. *Clin Radiol* 1994;49:485-9.
 21. Ogawa T, Suzuki T, Sakamoto M, Watanabe M, Tateda Y, Oshima T, Kato K, Sagai S, Kobayashi T, Shiga K. Correct diagnosis of Warthin tumor in the parotid gland with dynamic MRI. *Tohoku J Exp Med* 2012;227:53-7.
 22. Stefanovic X, Al Tabaa Y, Gascou G, Lacombe S, Auge Y, Delort P, Hagen P, Garrel R, Bonafe A, Daures JP, Vendrell JF. Magnetic Resonance Imaging of Parotid Gland Tumors: Dynamic Contrast-Enhanced Sequence Evaluation. *J Comput Assist Tomogr* 2017;41:541-6.
 23. Elmokadem AH, Abdel Khalek AM, Abdel Wahab RM, Tharwat N, Gaballa GM, Elata MA, Amer T. Diagnostic Accuracy of Multiparametric Magnetic Resonance Imaging for Differentiation Between Parotid Neoplasms. *Can Assoc Radiol J* 2019;70:264-72.
 24. Xiang S, Ren J, Xia Z, Yuan Y, Tao X. Histogram analysis of dynamic contrast-enhanced magnetic resonance imaging in the differential diagnosis of parotid tumors. *BMC Med Imaging* 2021;21:194.
 25. Liu YJ, Lee YH, Chang HC, Chung HW, Wang CW, Juan CH, Chu YH, Lee JC, Juan CJ. Imaging quality of PROPELLER diffusion-weighted MR imaging and its diagnostic performance in distinguishing pleomorphic adenomas from Warthin tumors of the parotid gland. *NMR Biomed* 2020;33:e4282.
 26. Karaman CZ, Tanyeri A, Özgür R, Öztürk VS. Parotid gland tumors: comparison of conventional and diffusion-weighted MRI findings with histopathological results. *Dentomaxillofac Radiol* 2021;50:20200391.
 27. Shao S, Zheng N, Mao N, Xue X, Cui J, Gao P, Wang B. A triple-classification radiomics model for the differentiation of pleomorphic adenoma, Warthin tumour, and malignant salivary gland tumours on the basis of diffusion-weighted imaging. *Clin Radiol* 2021;76:472.e11-8.
 28. Bruvo M, Mahmood F. Apparent diffusion coefficient measurement of the parotid gland parenchyma. *Quant Imaging Med Surg* 2021;11:3812-29.
 29. Gabelloni M, Faggioni L, Attanasio S, Vani V, Goddi

- A, Colantonio S, Germanese D, Caudai C, Bruschini L, Scarano M, Seccia V, Neri E. Can Magnetic Resonance Radiomics Analysis Discriminate Parotid Gland Tumors? A Pilot Study. *Diagnostics (Basel)* 2020;10:900.
30. Sarioglu O, Sarioglu FC, Akdogan AI, Kucuk U, Arslan IB, Cukurova I, Pekcevik Y. MRI-based texture analysis to differentiate the most common parotid tumours. *Clin Radiol* 2020;75:877.e15-23.
31. Gündüz E, Alçin ÖF, Kizilay A, Piazza C. Radiomics and deep learning approach to the differential diagnosis of parotid gland tumors. *Curr Opin Otolaryngol Head Neck Surg* 2022;30:107-13.
32. Hu Z, Guo J, Feng J, Huang Y, Xu H, Zhou Q. Value of T2-weighted-based radiomics model in distinguishing Warthin tumor from pleomorphic adenoma of the parotid. *Eur Radiol* 2023;33:4453-63.
33. Zhang G, Zhu L, Huang R, Xu Y, Lu X, Chen Y, Li C, Lei Y, Luo X, Li Z, Yi S, He J, Zheng C. A deep learning model for the differential diagnosis of benign and malignant salivary gland tumors based on ultrasound imaging and clinical data. *Quant Imaging Med Surg* 2023;13:2989-3000.
34. Matsusue E, Fujihara Y, Matsuda E, Tokuyasu Y, Nakamoto S, Nakamura K, Ogawa T. Differentiating parotid tumors by quantitative signal intensity evaluation on MR imaging. *Clin Imaging* 2017;46:37-43.
35. Pietragalla M, Nardi C, Bonasera L, Mungai F, Taverna C, Novelli L, De Renzis AGD, Calistri L, Tomei M, Occhipinti M, Colagrande S. The role of diffusion-weighted and dynamic contrast enhancement perfusion-weighted imaging in the evaluation of salivary glands neoplasms. *Radiol Med* 2020;125:851-63.

Cite this article as: He SN, Lu RC, Zhou JL, Wang B, Bi GL, Wu KH. Semiquantitative magnetic resonance imaging parameters for differentiating parotid pleomorphic adenoma from Warthin tumor. *Quant Imaging Med Surg* 2023;13(9):6152-6163. doi: 10.21037/qims-22-1445